



Microstructure and properties of the GEWZ522K casting magnesium alloy based on the Mg–Gd–Nd–Y–Zn–Zr system

A.V. Koltygin, A.V. Pavlov, V.E. Bazhenov, O.D. Gnatyuk, I.I. Baranov, V.D. Belov

National University of Science and Technology “MISIS”
4 build 1 Leninskiy Prosp., Moscow, 119049, Russia

✉ Viacheslav E. Bazhenov (V.E.Bagenov@gmail.com)

Abstract: The article discusses the solidification and phase composition of the (wt.%) Mg–4.8Gd–2.1Nd–1.6Y–0.4Zn–0.6Zr (GEWZ522K) casting alloy. It is demonstrated that in the as-cast state, the alloy structure comprises primary zirconium particles, dendrites of the magnesium solid solution (α Mg), and eutectic intermetallic phases located between dendritic branches. Following solution heat treatment at $t = 530 \pm 5$ °C, the alloy transitions into a single-phase state and can be significantly strengthened through artificial aging after quenching. It is recommended to apply alloy aging at $t = 250$ °C for 8–10 h or at $t = 200$ °C for 15–18 h. This approach leads to the maximum strengthening of the alloy, with the best mechanical properties achieved for the alloy aged at $t = 250$ °C. Regardless of the aging method used, the ultimate tensile strength (UTS) of the samples surpasses 300 MPa, which significantly exceeds that of commercial casting alloys according to GOST 2856–79. The measured corrosion rate for the GEWZ522K alloy is 7.5 ± 0.4 mm/year, that slightly higher than that for the less alloyed commercial alloy ML10 (approximately 2.5 mm/year) tested under similar conditions. Furthermore, the alloy was subjected to tests for ignition resistance when in contact with air. It was observed that with continuous airflow over the specimen's surface, ignition centers appear at $t = 625$ °C due to the breakdown of the oxide film, causing the alloy to nearly completely melt. Therefore, the GEWZ522K alloy can be employed as a high-strength casting alloy. However, during the operation of cast parts, particular attention must be paid to safeguarding the surface of these parts against corrosion.

Keywords: magnesium alloy, casting, Mg–Gd–Nd–Y–Zn–Zr, high strength alloy, magnesium corrosion, magnesium ignition.

For citation: Koltygin A.V., Pavlov A.V., Bazhenov V.E., Gnatyuk O.D., Baranov I.I., Belov V.D. Microstructure and properties of the GEWZ522K casting magnesium alloy based on the Mg–Gd–Nd–Y–Zn–Zr system. *Izvestiya. Non-Ferrous Metallurgy*. 2023;29(5):34–46. <https://doi.org/10.17073/0021-3438-2023-5-34-46>

Структура и свойства литейного магниевого сплава GEWZ522K системы Mg–Gd–Nd–Y–Zn–Zr

А.В. Колтыгин, А.В. Павлов, В.Е. Баженов, О.Д. Гнатюк, И.И. Баранов, В.Д. Белов

Национальный исследовательский технологический университет «МИСИС»
119049, Россия, г. Москва, Ленинский пр-т, 4, стр. 1

✉ Вячеслав Евгеньевич Баженов (V.E.Bagenov@gmail.com)

Аннотация: Рассмотрены кристаллизация и фазовый состав литейного сплава (мас.%) Mg–4,8Gd–2,1Nd–1,6Y–0,4Zn–0,6Zr (GEWZ522K). Показано, что в литом состоянии структура сплава состоит из первичных частиц циркония, дендритов магниевого твердого раствора α Mg и эвтектических интерметаллических фаз, находящихся между их ветвями. В результате отжига при

$t = 530 \pm 5$ °C сплав переходит в однофазное состояние и после закалки может быть значительно упрочнен в результате искусственного старения. Было предложено проводить старение сплава при $t = 250$ °C длительностью 8–10 ч или при $t = 200$ °C в течение 15–18 ч. При этом достигается максимальное упрочнение сплава, однако лучшие механические свойства были получены для сплава, состаренного при $t = 250$ °C. Независимо от режима старения, предел прочности на растяжение (σ_b) образцов превосходит 300 МПа, что гораздо выше показателей промышленных литейных сплавов по ГОСТ 2856–79. Рассчитанная скорость коррозии для сплава GEWZ522K равна $7,5 \pm 0,4$ мм/год, что несколько больше, чем для менее легированного промышленного сплава МЛ10 (порядка 2,5 мм/год), испытанного в аналогичных условиях. Сплав был также испытан на сопротивление к возгоранию в контакте с воздухом. Установлено, что при непрерывном поступлении воздуха к поверхности образца очаги возгорания появляются при $t = 625$ °C вследствие разрушения оксидной пленки, когда сплав практически полностью расплавляется. Таким образом, сплав GEWZ522K может быть использован в качестве высокопрочного литейного сплава. Однако при эксплуатации литых деталей из него необходимо уделять пристальное внимание защите их поверхности от коррозионного воздействия.

Ключевые слова: магниевый сплав, литье, Mg–Gd–Nd–Y–Zn–Zr, высокопрочный, коррозия магния, возгорание магния.

Для цитирования: Колтыгин А.В., Павлов А.В., Баженов В.Е., Гнатюк О.Д., Баранов И.И., Белов В.Д. Структура и свойства литейного магниевого сплава GEWZ522K системы Mg–Gd–Nd–Y–Zn–Zr. *Известия вузов. Цветная металлургия*. 2023;29(5):34–46. <https://doi.org/10.17073/0021-3438-2023-5-34-46>

Introduction

Magnesium alloys are considered one of the most promising materials for aerospace and automotive parts due to their low density, high specific strength, and high machining performance [1–3]. Nevertheless, despite the significant efforts made in recent decades to improve Mg alloys [4], their use remains very limited. One of the reasons for this limitation is the relatively low operating temperature of the most common industrial magnesium alloys and the associated fire in air [5; 6]. Additionally, due to magnesium's high chemical reactivity, magnesium alloys often exhibit reduced corrosion resistance [7].

It is well-known that the addition of rare earths (REs) to Mg-based alloys can significantly enhance their mechanical properties at both room and elevated operating temperatures, primarily through strengthening via artificial aging of a supersaturated solid solution of alloying elements in magnesium [3]. Neodymium is among the most commonly used rare earth element for alloying magnesium alloys. It is present in substantial quantities in industrial magnesium alloys hardened by aging. Its solubility decreases notably from approximately 2.1 wt.% at the eutectic temperature to very low values at room temperature [7; 8]. Yttrium also exhibits relatively high solubility in magnesium (~10 wt.%) and is frequently employed as an alloying component, particularly in alloys designed for elevated-temperature applications [5; 8–10]. The heavy rare-earth element gadolinium boasts substantial solubility in solid magnesium (~24 wt.%) at temperatures near the eutectic point. However, its solubility sharply decreases to 3.8 wt.% when the temperature is reduced to 200 °C, leading to significant strengthening during aging [10; 11]. The use of these rare earth elements for strengthening mag-

nesium-based alloys and extending their service temperature limit holds great promise.

Currently, several experimental alloys based on the Mg–Gd–Y–Zn–Zr system are known [12–14]. However, these alloys typically contain a high Gd content, exceeding 8 wt.%. This high Gd content is a consequence of the wide solubility range of gadolinium in solid magnesium. Nevertheless, by incorporating other rare earth elements (REs) such as neodymium into the alloy composition, it becomes possible to reduce the solubility of Gd and Y in magnesium, thus minimizing their presence in the alloy while achieving the desired strengthening effect. The objective of this study was to investigate a novel high-strength casting magnesium alloy. This alloy contains a significant amount of gadolinium as the primary alloying addition, alongside traditional neodymium and yttrium, which are common components in commercial casting alloys. The study focuses on the formation of the cast and heat-treated microstructure and phase composition of this new magnesium alloy [15], based on the Mg–Gd–Nd–Y–Zn–Zr system. By harnessing both light (Nd, Y) and heavy (Gd) rare earth elements, this alloy demonstrates impressive strength properties at relatively low concentrations of Gd and Y. Additionally, the study assesses the impact of these rare earth elements on the alloy's corrosion resistance and its susceptibility to ignition in air.

Materials and methods

The Mg–4.8Gd–2.1Nd–1.6Y–0.4Zn–0.6Zr (wt.%) alloy, designated as GEWZ522K, was prepared using the following materials: industrial-grade magnesium

(99.9 wt.% purity), zinc (99.975 wt.%), commercial master alloys Mg–15Zr (SOMZ LLC, Solikamsk), Mg–20Y, Mg–20Nd (Metagran PC, Moscow), and a Mg–36Gd (wt.%) master alloy produced in-house.

The Mg–Gd master alloy was fabricated in a resistance furnace using the flux free melting method. Initially, industrial-grade magnesium of 99.95 wt.% purity was placed in a clean steel crucible. After complete melting of magnesium, bulk gadolinium 99.9 wt.% purity was added to the melt. The melting process continued until the gadolinium was entirely dissolved. The resulting melt was poured into the mold at a temperature of 740 °C.

The alloy itself was prepared in a resistance furnace also using the flux free melting method. Melting took place in a PT 90/13 furnace (LAC, Czech Republic), within a steel crucible, under the protection of a mixture of argon and sulfur hexafluoride (SF₆) (2 vol.%). The process began with loading industrial-grade magnesium into a clean steel crucible, followed by the addition of zinc, Mg–Zr, Mg–Nd, Mg–Gd, and Mg–Y master alloys as the magnesium melted. After the melt reached a temperature of 780 °C, it was thoroughly mixed using a steel tool. The total mass of the molten alloy was 2 kg. Casting into molds occurred after a 15-minute hold in the furnace at a temperature of 760 °C. Subsequently, the crucible was removed from the furnace, and the alloy was cast into both steel and graphite molds once the melt temperature reached a temperature of 740 °C. The mold temperature was maintained at 25±2 °C. For microstructure analysis, corrosion tests, and ignition tests, cylindrical ingots 35 mm in diameter and 150 mm in height were cast into steel molds. To determine mechanical properties, the ingots were cast into graphite molds. After undergoing heat treatment, which included solution heat treatment followed by quenching and artificial aging (T6 mode), cylindrical proportional samples with a diameter of 5 mm (type III, number 7 according to GOST 1497-84) were cut from them. Details regarding the dimensions of the graphite mold and the sample cutting process can be found elsewhere [16].

The alloy's microstructure and phase composition were investigated using the Vega SBH3 scanning electron microscope (SEM) from Tescan (Czech Republic), equipped with the Oxford energy-dispersive X-ray spectroscopy attachment. Additionally, an Axio Observer D1m optical microscope (Carl Zeiss, Germany) was employed. An etchant solution comprising 11 g of picric acid, 11 mL of acetic acid, and 100 mL of ethyl alcohol was utilized to reveal the alloy's structure. To assess the chemical composition of the obtained alloys, energy dis-

persive X-ray spectroscopy (EDS) was performed within a 1×1 mm area.

Brinell hardness was determined using the NEMESIS 9001 universal hardness tester from INNOVATEST (Netherlands). The testing parameters included a 2.5 mm ball diameter, a 62.5 kgf load (≈613 N), and a 10-second hold time under load. A minimum of 5 measurements were conducted for each specimen.

Tensile mechanical properties were studied using the 5569 universal testing machine (Instron, USA), equipped with a non-contact video extensometer of AVE type (Instron, USA). Cylindrical samples with a 5 mm diameter (type III, No. 7 as per GOST 1497-84) were machined from blanks. The ram speed was set at 5 mm/min, and mechanical properties were determined based on at least 3 samples for each series of measurements.

Electrical conductivity measurements were conducted using the contact-free eddy current conductivity meter VE-27NC/4-5 from Sigma SPE, Ekaterinburg, with measurement limits of 5–37 MS/m. A minimum of 5 measurements were taken for each specimen.

Polythermal and isothermal sections of phase diagrams, the phase composition of alloys, and alloy solidification according to the Scheil–Gulliver model were calculated using Thermo-Calc 2016a software [17], with the thermodynamic database TCMG4 (magnesium alloys database, version 4) being utilized [18].

For corrosion tests, samples in the form of approximately 12×12×12 mm cubes, with a surface area of ~9 cm², were cut from the ingots after heat treatment in the T6 mode. The corrosion rate was determined using the volumetric method, based on the measurement of the amount of hydrogen released during specimens corrosion. Tests were conducted in a 3 wt.% NaCl aqueous solution at room temperature for 48 h, using a minimum of 5 samples for each series. The volume of the solution used was 500 mL. Before immersion in the solution, the sample surfaces were cleaned with P320 grit sandpaper and degreased with ethyl alcohol. The amount of released hydrogen was converted to the mass loss of the sample based on the 1 mL H₂ = 1 mg Mg ratio [19], and the corrosion rate was calculated in mm/year following the standard method [20].

To determine the ignition temperature, samples with dimensions of 25×25×60 mm were prepared. Their surfaces were cleaned using P320 grit paper. During the tests, the alloy sample was placed in a sealed steel crucible, and a constant airflow of 1 L/min, controlled by a rotameter, was provided in the crucible space. The crucible containing the sample was heated in a re-

sistance furnace to the desired temperature (600, 625, and 650 °C), with a subsequent 2-hour hold at that temperature. Temperature readings were recorded using the BTM-4208SD 12-channel temperature recorder (Lutron, Israel).

Results and discussion

Figure 1 depicts the microstructure of the alloy in as cast state. The predominant features include dendrites of a magnesium-based solid solution, within which precipitates of the second phase, formed through the eutectic reaction, are situated. Additionally, within the solid solution, distinct near spherical precipitates were identified in the microstructure using optical microscopy after etching. These precipitates exhibit significant contrast compared to the surrounding background when observed through SEM. To elucidate the phase composition of the alloy, its solidification behavior was analyzed by referencing the sections of the multicomponent phase diagram within the alloy's existence region. These calculations were performed using Thermo-Calc software. Zinc was not considered in the calculation due to its minimal presence in the alloy, which has an insignificant impact on the solidification process.

Figure 2 displays polythermal sections of the phase diagram within the composition region of the GEWZ522K alloy. It is evident that the equilibrium solidification process of the alloy starts with the precipi-

itation of primary zirconium-based crystals from the liquid at $t \sim 820$ °C. Thermo-Calc software calculations have indicated that these crystals are nearly pure zirconium. Subsequently, as the alloy temperature decreases to $t \sim 640$ °C, the peritectic reaction commences, leading to the complete transformation of zirconium into a magnesium-based solid solution (α Mg). Upon further cooling to $t \sim 520$ °C, zirconium precipitated once more from the supersaturated α Mg, forming its distinct phase. Consequently, the equilibrium effective freezing range of the alloy, excluding the primary zirconium solidification region, spans approximately 120 °C. Additionally, as the temperature decreases further, a compositionally variable phase, $Mg_{41}RE_5$ precipitates from α Mg, primarily consisting of a mixture of Nd and Y, with a minimal Gd content. Around $t \sim 300$ °C, the formation of the gadolinium-rich phase $GdMg_5$ becomes evident. Notably, an increase in the Y content exceeding 2 wt.% and a decrease in the Nd content below 1.5 wt.% alter the solidification path of the alloy, leading it into the realm of forming the binary compound $Mg_{24}Y_5$. Consequently, it can be inferred that the GEWZ522K alloy may not endure prolonged holding at $t = 300$ °C or higher. At such temperatures, the hardening gadolinium-based particles dissolve into the α Mg solid solution. Therefore, the practical upper operating temperature limit for this alloy is expected to be lower.

Figure 3 displays the isothermal sections of the multicomponent phase diagram for the Mg–2Nd–0.5Zn–

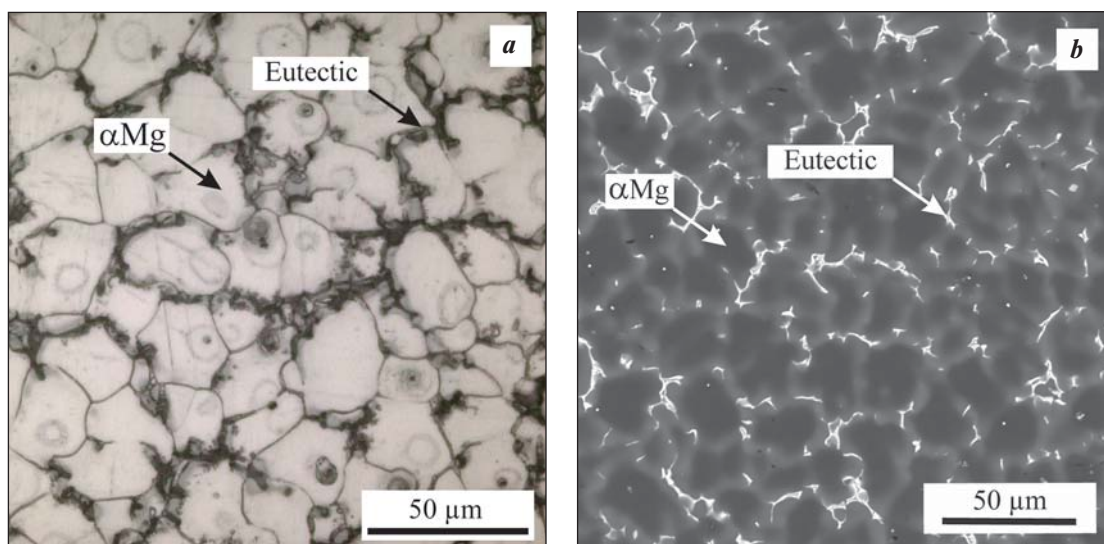


Fig. 1. Microstructure of the GEWZ522K alloy in the as-cast state
a – OM, etched; *b* – SEM

Рис. 1. Микроструктура сплава GEWZ522K в литом состоянии
a – ОМ, травлено; *b* – СЭМ

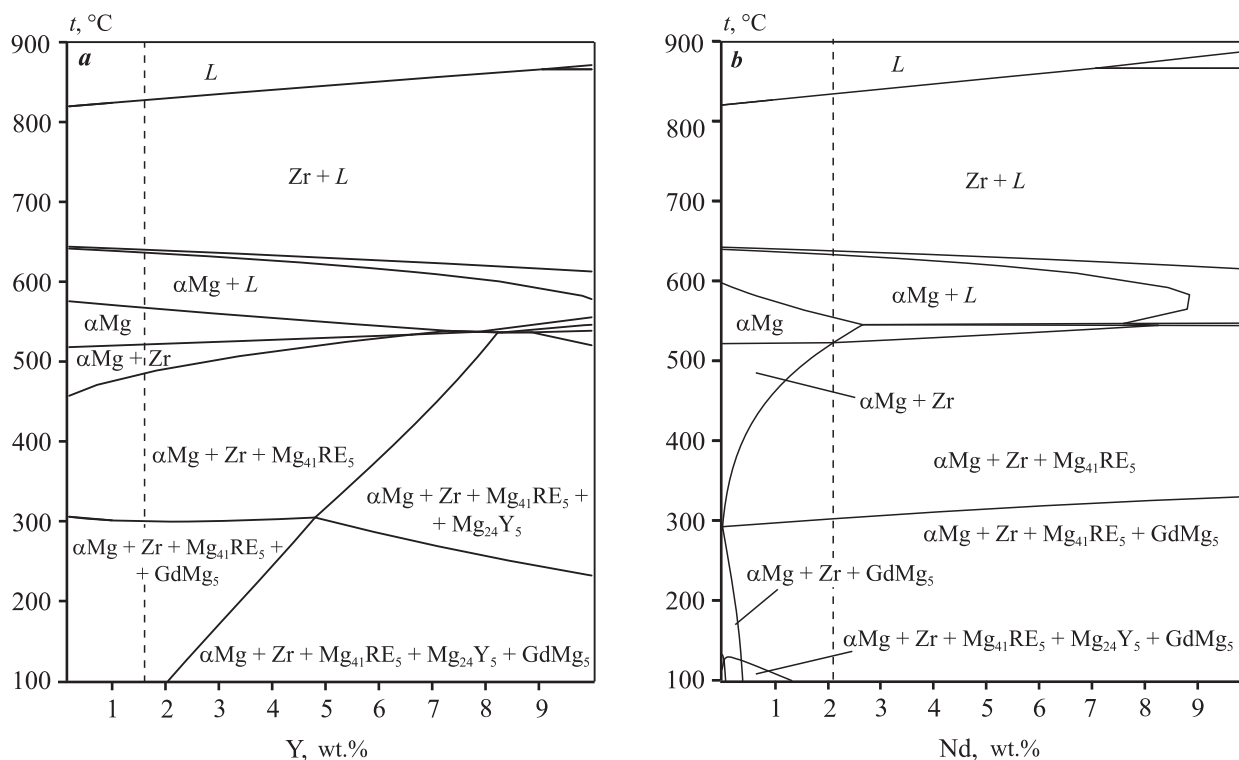


Fig. 2. Polythermal sections of the (wt.%) Mg–5Gd–2Nd–0.6Zr–Y (a) and Mg–5Gd–2Y–0.6Zr–Nd (b) phase diagrams. The dashed line shows the alloying components content in the GEWZ522K alloy.

Рис. 2. Политермические сечения диаграммы состояния для сплавов (мас.%) Mg–5Gd–2Nd–0,6Zr–Y (a) и Mg–5Gd–2Y–0,6Zr–Nd (b).

Пунктирной линией показано содержание легирующего компонента сплава GEWZ522K.

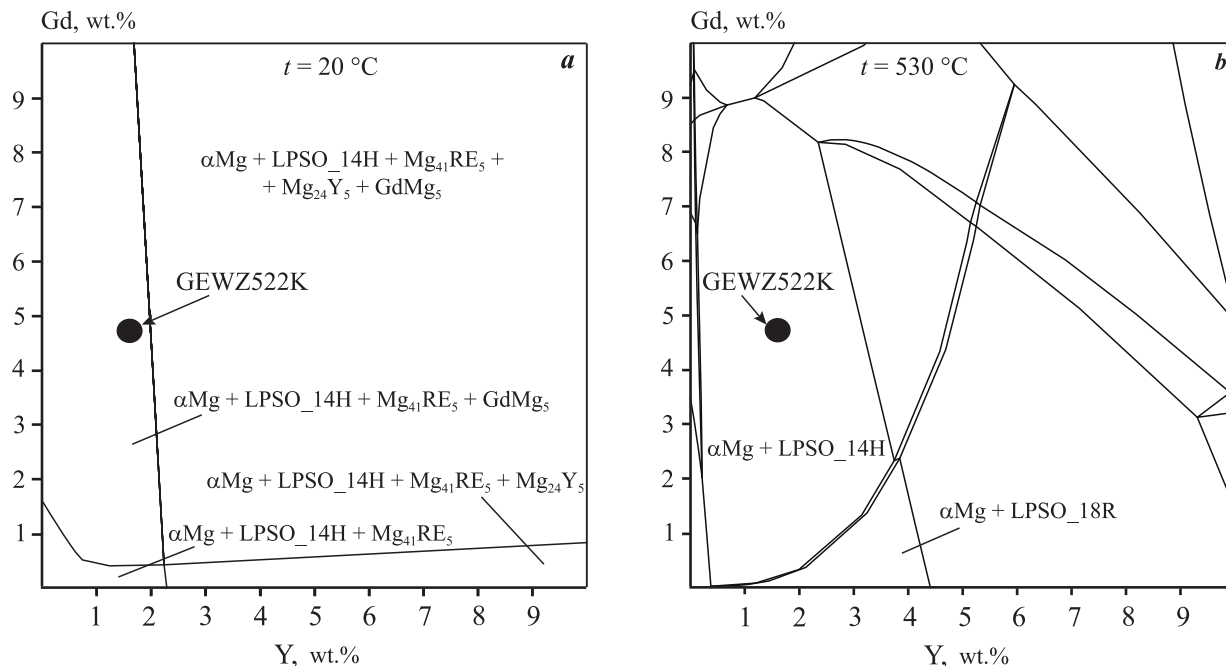


Fig. 3. Isothermal sections of the (wt.%) Mg–2Nd–0.5Zn–Y–Gd phase diagram at 20 °C (a) and 530 °C (b).

Рис. 3. Изотермические сечения диаграммы состояния сплава (мас.%) Mg–2Nd–0,5Zn–Y–Gd при температурах 20 °C (a) и 530 °C (b).

Y–Gd (wt.%) alloy at room temperature (20 °C) and at 530 °C, which is approximately 20 °C lower than the solidus temperature of the alloy (as shown in Fig. 2). In this calculation, zinc (0.5 %) was taken into account, and for the sake of clarity, zirconium was omitted. Notably, at $t = 530$ °C, the alloy exhibits a nearly single-phase equilibrium structure, with only a minimal presence of the LPSO phase. Despite our investigation of the as cast alloy's microstructure, the lamellar structure typically associated with LPSO was not observed. It is highly likely that this structure is either entirely absent or present in extremely low quantities.

Before proceeding with heat treatment, it is essential to confirm that the alloy does not form low melting point structural components or phases during non-equilibrium solidification. To assess this, solidification was calculated for the (wt.%) Mg–5.5Gd–2.0Nd–2.0Y–0.4Zn–0.6Zr alloy. This calculation employed slightly higher amounts of alloying elements to ensure the detection of potential non-equilibrium solidus temperature. As depicted in Fig. 4, the calculation employing the Scheil–Gulliver model reveals a non-equilibrium solidus at $t = 520$ °C. Nevertheless, the quantity of non-equilibrium phases formed at this temperature is negligible. To prevent the melting of the non-equilibrium eutectic, it is advisable to gradually reach the heat treatment temperature of 530 °C, allowing sufficient time for the dissolution of the non-equilibrium eutectic within α Mg.

At room temperature, the alloy exhibits equilibrium between the $Mg_{41}RE_5$ and $GdMg_5$ phases with the α Mg solid solution, possibly accompanied by a negligible presence of LPSO. Consequently, the alloy possesses the potential for heat treatment induced strengthening. This can be achieved by solution heat treatment at a temperature slightly below the solidus temperature, such as at $t = 530$ °C, followed by rapid quenching and subsequent aging. During aging, hardening particles enriched with REs are released, taking advantage of the known propensity of Gd alloys for artificial aging [10; 13]. Utilizing the polythermal section of the phase diagram obtained (refer to Fig. 2), it becomes possible to determine the appropriate aging temperature for the alloy within the temperature ranging from 200 to 250 °C. This temperature range corresponds to the region where hardening particles containing REs will precipitate from the α Mg supersaturated solution. Furthermore, the selection of the aging temperature took into consideration the anticipated maximum operating temperature of the cast component.

The alloy sample underwent a high-temperature solid solution heat treatment at $t = 530$ °C for 8 h, fol-

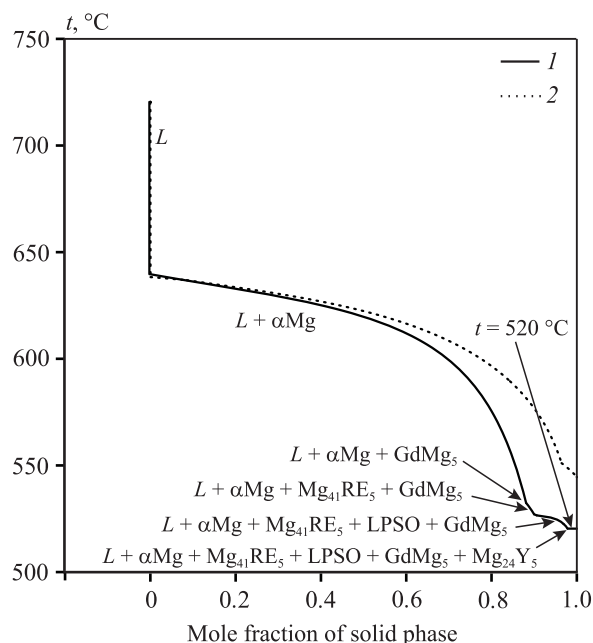


Fig. 4. Results of calculation of the solid phase fraction dependence on temperature for the Mg–5.5Gd–2.0Nd–2.0Y–0.4Zn–0.6Zr alloy at non-equilibrium solidification as per the Scheil–Gulliver model (1) and for equilibrium solidification conditions (2)

Рис. 4. Результаты расчета зависимости количества твердой фазы от температуры для сплава (мас.%) Mg–5,5Gd–2,0Nd–2,0Y–0,4Zn–0,6Zr при неравновесной кристаллизации по модели Шейла–Гулливера (1) и для равновесных условий кристаллизации (2)

lowed by quenching in hot water and subsequent aging at temperatures of $t = 200$ and 250 °C. The duration of the high-temperature solid solution heat treatment was determined based on the microstructure of the samples. Sufficient time was allowed for the dissolution of all eutectic intermetallic phases situated at the boundaries of α Mg dendrites. Figure 5 illustrates the resulting structure of the alloy after heat treatment, including solution heat treatment at $t = 530$ °C for 8 hours with water quenching, followed by aging at $t = 250$ °C for 9 h. Notably, all intermetallic phases present in the as cast structure along the α Mg dendrite boundaries have completely dissolved. Compact inclusions of the zirconium phase can be observed within the α Mg grains. Consequently, the alloy structure after heat treatment can be deemed single-phase. However, upon closer examination, micro-particles of the hardening phase can be observed, which formed as a result of the decomposition of the α Mg supersaturated solid solution during aging (Fig. 5, b). The largest and most distinct particles are prominently distributed around the zirconium inclusions.

The selection of the aging regime for the GEWZ522K alloy was based on the aim of achieving high mechanical properties after aging. During the aging process of alloys containing Gd and Y, hardening precipitates are sequentially formed as the α Mg supersaturated solid solution decomposes. This progression includes stages such as α Mg supersaturated solid solution \rightarrow metastable β'' (D019) \rightarrow metastable β' (cbco — base-centered orthorhombic lattice) \rightarrow metastable β_1 (fcc — face centered cubic lattice) \rightarrow stable β (fcc) [21; 22]. Importantly, the most significant hardening is accomplished by particles whose crystal lattice exhibits coherence or partial coherence with the lattice of the α Mg magnesium solid solution. Therefore, the maximum hardening occurs when the highest number of such particles is released. Since these particles are metastable, they gradually transition to a stable form and the hardening effect diminishes over time, a phenomenon known as the overaging effect. To determine the necessary aging duration for the alloy, samples after quenching were subjected to regular hardness measurements while being kept at the aging temperature. Hardness is directly related to the strength of the magnesium alloy: higher hardness corresponds to greater alloy strength. Consequently, the point at which maximum hardness is attained signifies optimal alloy hardening, and the time required to reach this hardness level represents the ideal aging duration at the given temperature.

Figure 6 illustrates the relationship between the hardness of the solution heat treated alloy and aging time at temperatures of $t = 200$ and 250 °C, with measurements conducted at 3-hour intervals. The results indicate that at $t = 250$ °C, maximum hardness is achieved after approximately 8 to 10 h of aging, with a decrease in hardness observed after $\tau = 12$ h. In the case of aging at $t = 200$ °C, maximum hardness is reached during a holding period of $\tau = 15\div 18$ h. These values for aging duration can be considered optimal for this alloy. The gradual precipitation in the supersaturated solid solution throughout the alloy aging process leads to a reduction in the concentration of alloying component atoms in magnesium. Consequently, this results in an increase in the electrical conductivity of the alloys during aging. Therefore, the change in electrical conductivity effectively correlates with the alteration in sample hardness during heat treatment and can serve as an additional indicator of the progress of the alloy aging process.

Tensile tests were conducted on the alloy after heat treatment, as depicted in Fig. 7. The results clearly demonstrate the alloy's impressive mechanical properties when compared to casting alloys commonly utilized in the native industry (according to GOST 2856-79). Regardless of the heat treatment process, the ultimate tensile strength (UTS) of the alloy consistently exceeded 300 MPa. Specifically, for the alloy aged at $t = 250$ °C,

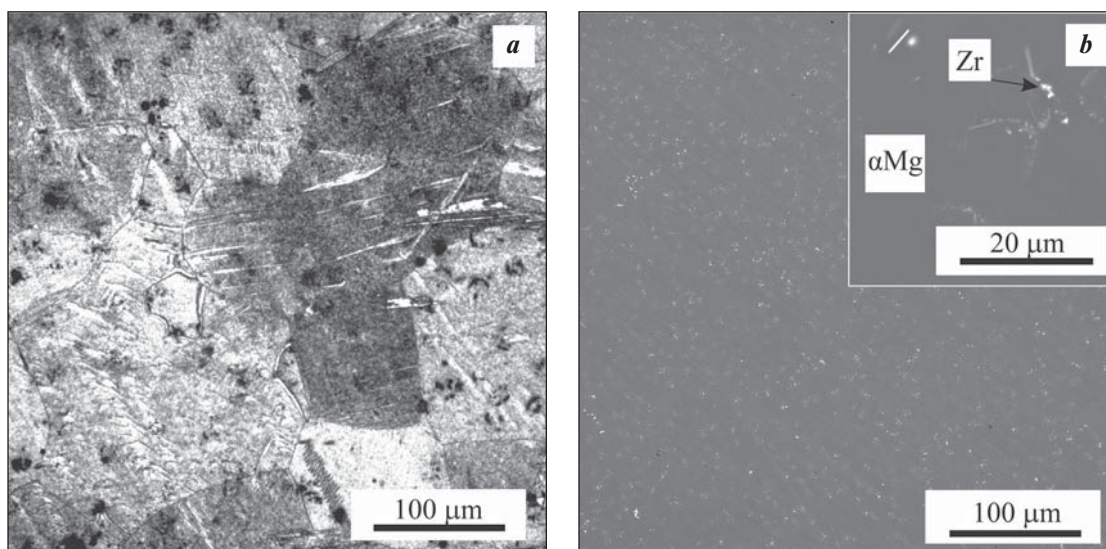


Fig. 5. Microstructure of the alloy after heat treatment (after solid solution treatment at $t = 530$ °C for 8 h with quenching, followed by aging at $t = 250$ °C for 9 h)

a – OM, etched; *b* – SEM

Рис. 5. Микроструктура сплава после термической обработки (закалка после отжига на твердый раствор при $t = 530$ °C в течение 8 ч с последующим старением при $t = 250$ °C в течение 9 ч)

a – ОМ, травлено; *b* – СЭМ

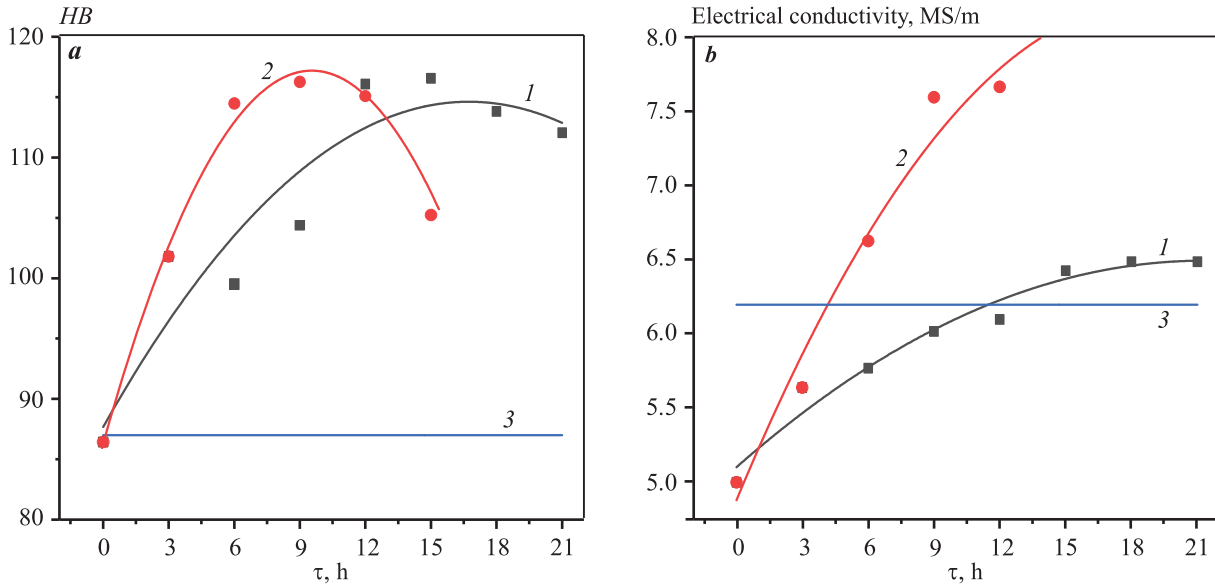


Fig. 6. Changes in hardness (a) and electrical conductivity (b) of the alloy during aging at $t = 200\text{ °C}$ (1) and 250 °C (2). The values for the as-cast state are given for comparison (3).

Рис. 6. Изменение твердости (a) и электропроводности (b) сплава в процессе старения при $t = 200\text{ °C}$ (1) и 250 °C (2). Для сравнения даны значения для литого состояния (3).

UTS = 325 ± 11 MPa, at $t = 200\text{ °C}$, UTS = 324 ± 4 MPa. These results are notable for magnesium alloys, surpassing the performance standards set by GOST 2856-79. The yield strength of the alloy after heat treatment also remained high, with values of 227 ± 6.5 MPa and 185 ± 21 MPa observed for alloys subjected to aging at $t = 250$ and 200 °C , respectively. In terms of elongation at fraction (EI), the studied samples that underwent aging at $t = 250$ and 200 °C exhibited values of $4.7 \pm 1.6\%$ and $3.3 \pm 0.4\%$, respectively. Consequently, the alloy aged at $t = 250\text{ °C}$ achieved the most favorable mechanical properties. It is worth noting that aging at $t = 200\text{ °C}$ did not yield similarly high mechanical properties within a reasonable time frame. The relatively wide confidence limits observed for the EI values of the studied alloys are attributed to the presence of oxide films, primarily comprised of Y and Gd. These films serve to protect the alloy from atmospheric contact and may also be introduced into the melt, ultimately remaining in the casting. This factor should be considered when developing production technologies, particularly when employing fluxfree melting methods that omit fluxes for melt treatment.

The study evaluating the corrosion behavior of the alloy in a NaCl solution was conducted to assess the corrosion resistance of this new material. Five samples were tested under identical conditions. As shown in Fig. 8, a, the samples exhibited very similar behavior during the tests. The calculated corrosion rate for the

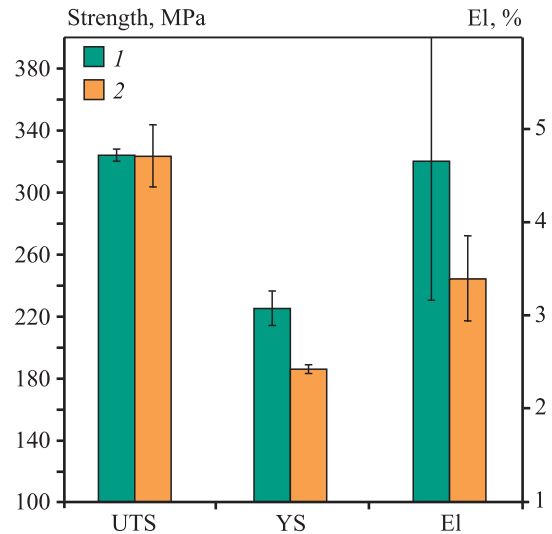


Fig. 7. Mechanical properties of the alloy after heat treatment 1 – solid solution treatment at 530 °C for 8 h + quenching + aging at 250 °C for 9 h; 2 – solid solution treatment at 530 °C for 8 h + quenching + aging at 200 °C for 16 h

Рис. 7. Механические свойства сплава после термической обработки 1 – отжиг на твердый раствор (530 °C , 8 ч) + закалка + старение (250 °C , 9 ч); 2 – отжиг на твердый раствор (530 °C , 8 ч) + закалка + старение (200 °C , 16 ч)

GEWZ522K alloy was determined to be 7.5 ± 0.4 mm/year, which is higher than that of the commercial alloy ML10 (approximately 2.5 mm/year) under similar test conditions [23]. This difference in corrosion rates may

be attributed to the abundance of hardening particles released within the magnesium solid solution during the aging process, which act as cathodes in relation to it. Consequently, numerous microgalvanic pairs are formed, intensifying galvanic corrosion [23; 24]. In Fig. 8, *b*, the cross-section of a sample after corrosion tests is presented. It can be observed that the most significant areas of corrosion damage in the alloy are located in regions where intermetallic phases and zirconium precipitates (indicated by white dots) accumulate. This suggests that their presence in the alloy structure exacerbates corrosion. Notably, the ML10 commercial alloy contains up to 2.8 wt.% of Nd, whereas the studied GEWZ522K alloy contains a sum of 8.5 wt.% REs. This threefold increase in the total RE content in the studied alloy led to a corresponding threefold increase in the corrosion rate compared to the ML10 alloy. This observation confirms the notion of an almost linear correlation between the galvanic corrosion rate of heat-treated alloys with REs and Zr and the total content of REs and Zr [23]. Consequently, an increase in the corrosion rate in RE-rich alloys is an unavoidable trade-off for enhancing the alloy's mechanical properties. The introduction of elements that form a more robust layer of corrosion products on the alloy's surface in corrosive environments could potentially reduce the corrosion rate, but further research is necessary to explore this avenue.

The propensity of the cast magnesium alloy to ignite in the presence of air is of paramount importance. The addition of yttrium and gadolinium was expected to raise the ignition temperature of the alloy under examination. Flammability tests were conducted on the alloy samples. The methodology employed in this study allowed for some degree of simulation of actual conditions in which magnesium parts might ignite, as the alloy samples were consistently exposed to air blowing over their surface. The results indicated that the alloy resisted ignition until it reached complete melting, at which point the surface oxide film broke. As shown in Fig. 9, under the conditions of sample heating to a temperature of 625 °C, isolated ignition centers appeared, accompanied by significant deviations in the temperature curve, indicating substantial heat release. This behavior stemmed from variations in the geometry of the samples and the disruption of the protective oxide film on their surface. The presence of yttrium and gadolinium in the alloy led to the formation of a relatively dense surface oxide film that protected the alloy from oxidation [25; 26]. When the samples melted and underwent changes in geometry, the existing oxide film on the alloy's surface lost continuity and failed to regenerate under the experimental conditions, resulting in the emergence of ignition centers. Therefore, it can be concluded that the alloy demonstrates notable resistance to ignition, at least until complete melting occurs.

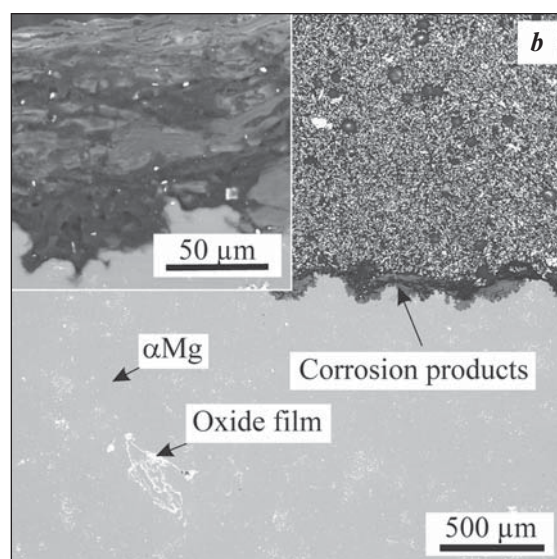
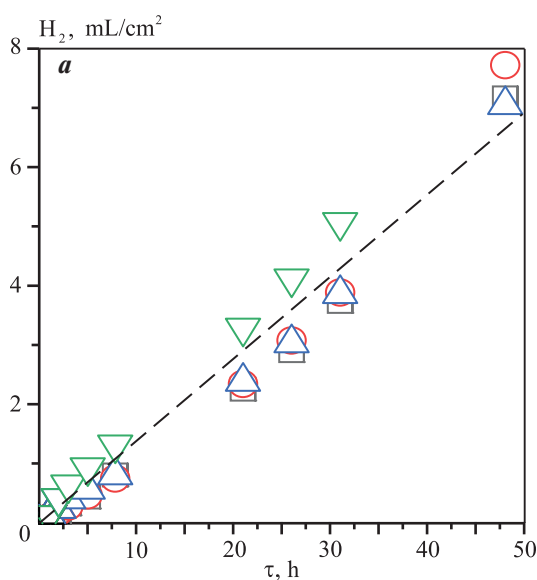


Fig. 8. Dependence of hydrogen evolution on the corrosion test time of alloy samples in 3 wt.% NaCl aqueous solution at room temperature for 48 h (the dashed line shows the averaged dependence) (*a*) and cross-section of the sample after corrosion tests (*b*)

Рис. 8. Зависимость выделения водорода от времени коррозионных испытаний образцов сплава в водном растворе 3 мас.% NaCl при комнатной температуре в течение 48 ч (штриховая линия – усредненная зависимость) (*a*) и поперечное сечение образца после коррозионных испытаний (*b*)

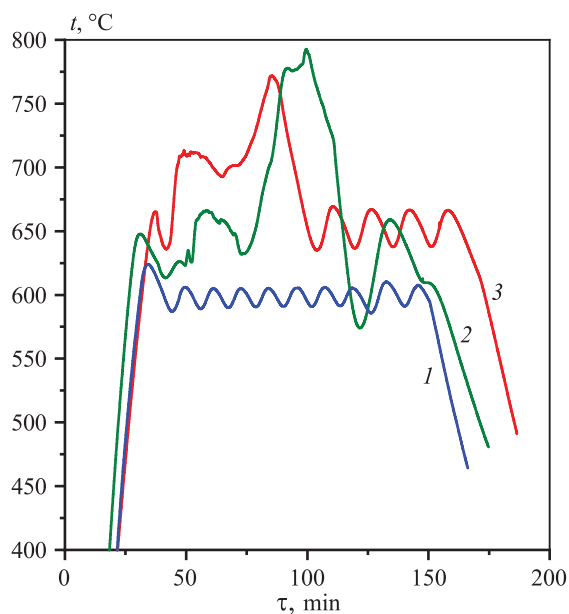


Fig. 9. Ignition test for the GEWZ522K alloy in air at $t = 600\text{ }^{\circ}\text{C}$ (1), $625\text{ }^{\circ}\text{C}$ (2), $650\text{ }^{\circ}\text{C}$ (3)

Рис. 9. Испытание на возгорание для сплава GEWZ522K на воздухе при $t = 600\text{ }^{\circ}\text{C}$ (1), $625\text{ }^{\circ}\text{C}$ (2), $650\text{ }^{\circ}\text{C}$ (3)

Conclusions

1. The structure of the GEWZ522K casting alloy comprises αMg -based solid solution dendrites and eutectic intermetallic phases situated between these dendritic branches. Furthermore, the alloy's structure features small zirconium precipitates formed as soon as the alloy's temperature drops below the liquidus. Simultaneously, the alloy exhibits an equilibrium freezing range of approximately $120\text{ }^{\circ}\text{C}$, which is shorter than that of most commercial casting magnesium alloys as per GOST 2856-79. The alloy's structure includes two types of intermetallics containing rare earth elements (REs): $\text{Mg}_{41}\text{RE}_5$, primarily composed of a mixture of Nd and Y, and GdMg_5 , which predominantly contains gadolinium.

2. The optimal solution heat treatment temperature for the alloy to reach single phase structure has been determined as $530 \pm 5\text{ }^{\circ}\text{C}$. At this temperature, nearly all phases except Zr completely dissolve in αMg . The duration of solution heat treatment depends on the thickness of the casting and typically lasts around 8–10 h. Subsequent to quenching, the alloy can undergo aging, during which metastable and stable hardening particles containing REs are formed. However, calculations for a completely non-equilibrium solidification, following the Scheil–Gulliver model, suggest a non-equilibrium solidus temperature of

$520\text{ }^{\circ}\text{C}$. This should be taken into consideration when designing the heat treatment regime to prevent melting of the non-equilibrium eutectic.

3. The alloy experiences significant strengthening through heat treatment in the T6 mode. The best strengthening results are achieved at an aging temperature of $250\text{ }^{\circ}\text{C}$. Under these conditions, the alloy exhibits a high yield strength of $\text{YS} = 227 \pm 6.5\text{ MPa}$, with a elongation at fracture of $\text{El} = 4.7 \pm 1.6\%$. The tensile strength of the alloy remains around $\text{UTS} \sim 325\text{ MPa}$, regardless of the aging temperature. The alloy's hardness after aging is approximately 110 HB.

4. Post-heat treatment, the alloy's structure is primarily single-phase, representing a solid solution with microscopic strengthening particles formed through aging. Clusters of such particles, which are larger in size, are notably observed around the primary Zr crystals. The LPSO phase, predicted by calculations, has not been detected in significant quantities within the alloy structure.

5. The corrosion rate of the alloy post-heat treatment exceeds that of the commercial ML10 alloy, produced and tested under similar conditions. This difference is attributed to the threefold increase in the total RE content in the studied alloy compared to ML10, resulting in a larger number of cathode particles formed during alloy aging and exhibiting a greater total surface area. These particles form microgalvanic pairs with the magnesium-based solid solution, leading to galvanic corrosion in the electrolyte medium.

6. Under continuous air exposure to the specimen's surface, ignition centers emerge at temperatures of $t = 625\text{ }^{\circ}\text{C}$. In this scenario, yttrium and gadolinium within the alloy are consumed in the formation of a dense oxide film on the metal surface.

References

1. Weiler J.P. A review of magnesium die-castings for closure applications. *Journal of Magnesium and Alloys*. 2019;7(2):297–304. <https://doi.org/10.1016/j.jma.2019.02.005>
2. Kulekci M.K. Magnesium and its alloys applications in automotive industry. *The International Journal of Advanced Manufacturing Technology*. 2008;39:851–865. <https://doi.org/10.1007/s00170-007-1279-2>
3. Zhang J., Liu S., Wu R., Hou L., Zhang M. Recent developments in high-strength Mg–RE-based alloys: Focusing on Mg–Gd and Mg–Y systems. *Journal of Magnesium and Alloys*. 2018;6(3):277–291. <https://doi.org/10.1016/j.jma.2018.08.001>

4. Yang Y., Xiong X., Chen J., Peng X., Chen D., Pan F. Research advances in magnesium and magnesium alloys worldwide in 2020. *Journal of Magnesium and Alloys*. 2021;9(3):705–747.
<https://doi.org/10.1016/j.jma.2021.04.001>
5. Fan J.F., Yang Ch.L., Han G., Fang S., Yang W.D., Xu B.S. Oxidation behavior of ignition-proof magnesium alloys with rare earth addition. *Journal of Alloys and Compounds*. 2011;509(5):2137–2142.
<https://doi.org/10.1016/j.jallcom.2010.10.168>
6. Aydin D.S., Bayindir Z., Hoseini M., Pekguleryuz M.O. The high temperature oxidation and ignition behavior of Mg–Nd alloys. Part I: The oxidation of dilute alloys. *Journal of Alloys and Compounds*. 2013;569: 35–44.
<https://doi.org/10.1016/j.jallcom.2013.03.130>
7. Morozova G.I. Phase composition and corrosion resistance of magnesium alloys. *Metal Science and Heat Treatment*. 2008;50:100–104.
<https://doi.org/10.1007/s11041-008-9020-9>
Морозова Г.И. Фазовый состав и коррозионная стойкость магниевых сплавов. *Металловедение и термическая обработка металлов*. 2008;3(633):8–12.
8. Rokhlin L.L., Dobatkina T.V., Tarytina I.E., Timofeev V.N., Balakhchi E.E. Peculiarities of the phase relations in Mg-rich alloys of the Mg–Nd–Y system. *Journal of Alloys and Compounds*. 2004;367(1-2):17–19.
<https://doi.org/10.1016/j.jallcom.2003.08.004>
9. Rokhlin L.L. Magnesium alloys containing rare earth metals: Structure and properties. 1st ed. London: CRC Press, 2003. 256 p. <https://doi.org/10.1201/9781482265163>
10. Gao L., Chen R.S., Han E.H. Effects of rare-earth elements Gd and Y on the solid solution strengthening of Mg alloys. *Journal of Alloys and Compounds*. 2009;481(1-2): 379–384.
<https://doi.org/10.1016/j.jallcom.2009.02.131>
11. Stulikova I., Smola B., Cizek J., Kekule T., Melikhova O., Kudrnova H. Natural and artificial aging in Mg–Gd binary alloys. *Journal of Alloys and Compounds*. 2018;738:173–181.
<https://doi.org/10.1016/j.jallcom.2017.12.026>
12. Wei X., Jin L., Dong S., Wang F., Dong J. Effect of Zn/(Gd + Y) ratio on the microstructure evolution and mechanical properties of Mg–Gd–Y–Zn–Zr alloy. *Materials Characterization*. 2020;169:110670.
<https://doi.org/10.1016/j.matchar.2020.110670>
13. Zheng J., Yan Z., Ji J., Shi Y., Zhang H., Zhang Z., Xue Y. Effect of heat treatment on mechanical properties and microstructure evolution of Mg–9.5Gd–4Y–2.2Zn–0.5Zr alloy. *Journal of Magnesium and Alloys*. 2022;10(4): 1124–1132.
<https://doi.org/10.1016/j.jma.2021.05.018>
14. Liu W., Zhou B., Wu G., Zhang L., Peng X., Cao L. High temperature mechanical behavior of low-pressure sand-cast Mg–Gd–Y–Zr magnesium alloy. *Journal of Magnesium and Alloys*. 2019;7(4):597–604.
<https://doi.org/10.1016/j.jma.2019.07.006>
15. Koltygin A.V., Pavlov A.V., Bazhenov V.E., Belov V.D. High strength magnesium alloy: Patent 2786785 (RF). 2022. (In Russ.).
КОЛТЫГИН А.В., ПАВЛОВ А.В., БАЖЕНОВ В.Е., БЕЛОВ В.Д. Высокопрочный литейный магниевый сплав: Патент 2786785 (РФ). 2022.
16. Bazhenov V.E., Koltygin A.V., Sung M.C., Park S.H., Tselovalnik Yu.V., Stepashkin A.A., Rizhsky A.A., Belov M.V., Belov V.D., Malyutin K.V. Development of Mg–Zn–Y–Zr casting magnesium alloy with high thermal conductivity. *Journal of Magnesium and Alloys*. 2021;9(5):1567–1577.
<https://doi.org/10.1016/j.jma.2020.11.020>
17. Andersson J.O., Helander T., Höglund L., Shi P.F., Sundman B. Thermo-Calc and DICTRA, Computational tools for materials science. *CALPHAD*. 2002;26(2): 273–312.
[https://doi.org/10.1016/S0364-5916\(02\)00037-8](https://doi.org/10.1016/S0364-5916(02)00037-8)
18. Thermo-Calc software TCMG4: TCS Mg-based alloys database. Version 4. <https://thermocalc.com/products/databases/magnesium-based-alloys/> (accessed: 01.05.2022).
19. Kirkland N.T., Birbilis N., Staiger M.P. Assessing the corrosion of biodegradable magnesium implants: a critical review of current methodologies and their limitations. *Acta Biomaterialia*. 2012;8(3):925–936.
<https://doi.org/10.1016/j.actbio.2011.11.014>
20. ASTM Standard G1-03. Standard practice for preparing, cleaning, and evaluating corrosion test specimens. West Conshohocken: ASTM International, 2011.
21. Zhou B., Liu W., Wu G., Zhang L., Zhang X., Ji H., Ding W. Microstructure and mechanical properties of sand-cast Mg–6Gd–3Y–0.5Zr alloy subject to thermal cycling treatment. *Journal of Materials Science & Technology*. 2020;43:208–219.
<https://doi.org/10.1016/j.jmst.2020.01.013>
22. He S.M., Zeng X.Q., Peng L.M., Gao X., Nie J.F., Ding W.J. Precipitation in a Mg–10Gd–3Y–0.4Zr (wt.%)

- alloy during isothermal ageing at 250 °C. *Journal of Alloys and Compounds*. 2006;421(1-2):309–313.
<https://doi.org/10.1016/j.jallcom.2005.11.046>
23. Bazhenov V.E., Sannikov A.V., Saidov S.S., Rizhskii A.A., Koltygin A.V., Belov V.D., Yudin V.A. Effect of alloying elements content and cooling rate on corrosion resistance of ML10. *Liteinoe Proizvodstvo*. 2020;(12):13–18. (In Russ.).
 Баженов В.Е., Санников А.В., Саидов С.С., Рижский А.А., Колтыгин А.В., Белов В.Д., Юдин В.А. Влияние содержания легирующих элементов и скорости охлаждения на коррозионную стойкость сплава МЛ10. *Литейное производство*. 2020;(12):13–18.
24. Kubásek J., Vojtěch D. Structural and corrosion characterization of biodegradable Mg–RE (RE = Gd, Y, Nd) alloys. *Transactions of Nonferrous Metals Society of China*. 2013;23(5):1215–1225.
[https://doi.org/10.1016/S1003-6326\(13\)62586-8](https://doi.org/10.1016/S1003-6326(13)62586-8)
25. Bazhenov V.E., Baranov I.I., Lyskovich V.V., Koltygin A.V., Sannikov A.V., Kyaramyan K.A., Belov V.D., Pavlinich S.P. Investigation of castability, mechanical, corrosion properties and flammability of ML-OPB and EWZ43 magnesium alloys. *Izvestiya. Non-Ferrous Metallurgy*. 2023;29(1):39–55. (In Russ.).
<https://doi.org/10.17073/0021-3438-2023-1-39-55>
 Баженов В.Е., Баранов И.И., Лыскович А.А., Колтыгин А.В., Санников А.В., Кярамян К.А., Белов В.Д., Павлинич С.П. Исследование литейных, механических, коррозионных свойств и пожароопасности магневых сплавов МЛ-ОПБ и EWZ43. *Известия вузов. Цветная металлургия*. 2023;29(1):39–55. <https://doi.org/10.17073/0021-3438-2023-1-39-55>
26. Tekumalla S., Gupta M. An insight into ignition factors and mechanisms of magnesium based materials: A review. *Materials & Design*. 2017;113:84–98.
<https://doi.org/10.1016/j.matdes.2016.09.103>

Information about the authors

Andrey V. Koltygin – Cand. Sci. (Eng.), Assistant Prof., Department of Foundry Technologies and Material Art Working (FT&MAW), National University of Science and Technology “MISIS” (NUST MISIS).

<https://orcid.org/0000-0002-8376-0480>

E-mail: misistlp@mail.com

Aleksandr V. Pavlov – Postgraduate Student, Department of FT&MAW, NUST MISIS.

<https://orcid.org/0009-0001-1934-0107>

E-mail: pavloveone@mail.ru

Viacheslav E. Bazhenov – Cand. Sci. (Eng.), Assistant Prof., Department of FT&MAW, NUST MISIS.

<https://orcid.org/0000-0003-3214-1935>

E-mail: V.E.Bagenov@gmail.com

Olesya D. Gnatyuk – Student, Department of FT&MAW, NUST MISIS.

<https://orcid.org/0009-0005-5881-5135>

E-mail: olessyal234@mail.ru

Ivan I. Baranov – Student, Department of FT&MAW, NUST MISIS.

<https://orcid.org/0000-0002-0465-7865>

E-mail: baranov.wania@yandex.ru

Vladimir D. Belov – Dr. Sci. (Eng.), Head of the Department of FT&MAW, NUST MISIS.

<https://orcid.org/0000-0003-3607-8144>

E-mail: vdbelov@mail.ru

Информация об авторах

Андрей Вадимович Колтыгин – к.т.н., доцент кафедры литейных технологий и художественной обработки материалов (ЛТиХОМ) Национального исследовательского технологического университета «МИСИС» (НИТУ МИСИС).

<https://orcid.org/0000-0002-8376-0480>

E-mail: misistlp@mail.ru

Александр Валерьевич Павлов – аспирант кафедры ЛТиХОМ, НИТУ МИСИС.

<https://orcid.org/0009-0001-1934-0107>

E-mail: pavloveone@mail.ru

Вячеслав Евгеньевич Баженов – к.т.н., доцент кафедры ЛТиХОМ, НИТУ МИСИС.

<https://orcid.org/0000-0003-3214-1935>

E-mail: V.E.Bagenov@gmail.com

Олеся Дмитриевна Гнатюк – студент кафедры ЛТиХОМ, НИТУ МИСИС.

<https://orcid.org/0009-0005-5881-5135>

E-mail: olessyal234@mail.ru

Иван Ильич Баранов – студент кафедры ЛТиХОМ, НИТУ МИСИС.

<https://orcid.org/0000-0002-0465-7865>

E-mail: baranov.wania@yandex.ru

Владимир Дмитриевич Белов – д.т.н., заведующий кафедрой ЛТиХОМ, НИТУ МИСИС.

<https://orcid.org/0000-0003-3607-8144>

E-mail: vdbelov@mail.ru

Contribution of the authors

A.V. Koltygin – conceptualization, experimental data analysis, manuscript writing.

A.V. Pavlov – conducted experiments, analyzed experimental data.

V.E. Bazhenov – analyzed experimental data, edited the manuscript.

O.D. Gnatyuk – prepared samples, performed experiments.

I.I. Baranov – conducted experiments, analyzed experimental data.

V.D. Belov – supervision, manuscript editing.

Вклад авторов

А.В. Колтыгин – формирование основной концепции, обработка результатов исследований, написание текста статьи.

А.В. Павлов – проведение экспериментов, обработка результатов исследований.

В.Е. Баженов – обработка результатов исследований, редактирование текста статьи.

О.Д. Гнатыук – подготовка образцов, проведение экспериментов.

И.И. Баранов – проведение экспериментов, обработка результатов исследований.

В.Д. Белов – общее руководство, редактирование текста статьи.

The article was submitted 03.04.2023, revised 19.06.2023, accepted for publication 23.06.2023

Статья поступила в редакцию 03.04.2023, доработана 19.06.2023, подписана в печать 23.06.2023